



# Optics Letters

## High resolution, high channel count mid-infrared arrayed waveguide gratings in silicon

ADITYA MALIK,<sup>1,\*</sup>  ALEXANDER SPOTT,<sup>1,2</sup>  YUE WANG,<sup>1</sup> ERIC J. STANTON,<sup>3</sup>  JON PETERS,<sup>1</sup> AND JOHN E. BOWERS<sup>1</sup> 

<sup>1</sup>Department of Electrical & Computer Engineering, University of California Santa Barbara, Santa Barbara, California 93106, USA

<sup>2</sup>Current Address: Mirios Inc., Santa Barbara, California 93106, USA

<sup>3</sup>Applied Physics Division, National Institute of Standards and Technology, Boulder, Colorado 80305, USA

\*Corresponding author: amalik@ece.ucsb.edu

Received 8 May 2020; revised 20 June 2020; accepted 16 July 2020; posted 16 July 2020 (Doc. ID 397135); published 11 August 2020

Arrayed waveguide gratings (AWGs) working in the 4.7  $\mu\text{m}$  wavelength range are reported on silicon-on-insulator waveguides with 1500 nm thick silicon and 2  $\mu\text{m}$  thick buried oxide layers. For eight channel devices, three different channel spacings (200 GHz, 100 GHz, and 50 GHz) with cross talk levels of  $-32.31$  dB,  $-31.87$  dB, and  $-27.28$  dB and insertion loss levels of  $-1.43$  dB,  $-4.2$  dB, and  $-2.3$  dB, respectively, are demonstrated. Fourteen channel AWGs with 170 GHz channel spacing and 16 channel AWGs with 87 GHz channel spacing are shown to have a cross talk value of  $-21.67$  dB and  $-24.30$  dB and insertion loss value of  $-4.2$  dB and  $-3.8$  dB, respectively. Two AWGs with 10 nm difference in channel peak are designed, and the measurements show a 9.3 nm difference. The transmission spectrum shift as a function of temperature is found to be  $0.22$  nm/ $^{\circ}\text{C}$ . © 2020 Optical Society of America

<https://doi.org/10.1364/OL.397135>

Arrayed waveguide gratings (AWGs) are one of the most broadly implemented integrated optics components. They were developed in the C-band (centered around 1550 nm wavelength) and in the O-band (centered around 1300 nm wavelength) for applications in telecommunication transceiver networks and datacenters [1]. AWGs are mainly used either as wavelength (de)multiplexers to separate or combine individual wavelength channels or as switches to route light from one waveguide to the other. Today, silicon-on-insulator (SOI) waveguide circuits are the main workhorse for photonic integrated circuits (PICs) and SOI AWGs with low insertion loss and low cross talk have been reported [2–4]. The wavelength (de)multiplexing capabilities of AWGs make them an interesting candidate for other applications such as Raman spectroscopy [5], gas sensors [6,7], and astronomy [8]. AWGs can be deployed as spectrometers to detect different wavelength bands corresponding to the specific molecular species. A high resolution spectrometer with a high channel count is needed for efficient detection of individual gas lines of molecules or to detect overlapping gas lines of several molecular species at once. In the past few years, there have been several reports of AWGs working in the mid-infrared wavelength regime (i.e., beyond 2  $\mu\text{m}$  wavelength) based on silicon

[9,10], germanium [11,12], and SiGe [13,14] waveguides. The rationale behind developing AWGs beyond the telecommunication range stems from the interest in on-chip spectroscopic sensing. Fourier-transform-based spatial heterodyne spectrometers (SHSs) operating in the mid-infrared represent another class of recently reported mid-infrared spectrometers [15–18]. SHSs are constructed using several Mach-Zehnder interferometers (MZIs) connected in parallel to sample an incoming waveform. While they have a smaller footprint in comparison to AWGs, they also require precise phase control (usually in the form of thermo-optic phase shifters), and the total system becomes more complex. AWGs, on the other hand, are stand-alone passive components, and if designed properly, can be inserted in spectroscopic sensing systems without any additional control circuitry. A constant challenge in designing high performing SOI AWGs has been the cross talk associated with the phase errors accumulated from the rough side walls. This challenge is accentuated for cases where a high resolution or higher channel count is desired because both the number of arms in the waveguide array and the overall size increase for both these cases.

The previous reports of AWGs fabricated on thin SOI waveguides (device layer thickness  $<500$  nm) were limited in operational wavelength to 3.8  $\mu\text{m}$ . This upper limit on the SOI waveguides is imposed by the high absorption of the buried oxide (BOX) layer. To enable operation beyond 4  $\mu\text{m}$ , either the BOX layer needs to be removed locally [19] or the silicon device layer thickness can be increased to reduce the modal overlap with the BOX layer [20,21]. Both approaches have shown low propagation losses; however, the second approach is more favorable for realizing integrated lasers on SOI waveguides from a thermal and mechanical point of view [22,23]. In this Letter, we report on low cross talk silicon AWGs working near 4.7  $\mu\text{m}$  wavelength range. The silicon waveguide thickness is 1500 nm, and the BOX layer is 2  $\mu\text{m}$  thick. While this waveguide platform does provide low loss transmission in this wavelength range, it is not currently offered by any commercial SOI pilot line. For eight channel devices, three different resolutions (200 GHz, 100 GHz, 50 GHz) are reported. We also show devices with 14 and 16 channels with resolution 160 GHz and 87 GHz, respectively. Table 1 shows the performance of mid-infrared AWGs fabricated in various material systems in terms of number

**Table 1. Comparison of Mid-IR AWGs**

Material System	$N_{\text{ch}}$	$\Delta\lambda$ (GHz)	Cross Talk (dB)
SOI [9]	8	200	-23.15
SOI [23]	8	300	-14
Ge-on-Si [12]	8	200	-29.63
SiGe-on-Si [13]	15	88.2	-20
SiGe-on-Si [14]	18	90	-20
SOI (This Work)	8	200/50	-32.31/-27.28
SOI (This Work)	16	87	-24.3

of channels ( $N_{\text{ch}}$ ), channel spacing ( $\Delta\lambda$ ), and cross talk level. For eight channel devices, the cross talk level is superior than previously published results even for a higher resolution of 50 GHz. The robust design ensures that even for a higher channel count, the measured cross talk levels show an improvement over previously published results. We had previously reported SOI AWGs on same waveguide platform with 300 GHz resolution and eight channels [23]. These devices were used to show the beam combination properties of AWGs. Even for such coarse resolution, the measured cross talk value was found to be -14 dB. The higher cross talk arises because (a) the width of the array waveguide ( $w_{\text{AWG}}$ ) was kept at 1.5  $\mu\text{m}$ , which made it more susceptible to phase errors arising from side wall scattering, and (b) various AWG design parameters were not fully optimized. In this manuscript, we have designed AWGs with much finer resolution (as high as 50 GHz) and higher channel count (16). By carefully choosing the AWG design parameters (as detailed later) and by choosing  $w_{\text{AWG}}$  to be 4  $\mu\text{m}$  wide, we reduced the cross talk levels even for higher resolution devices. We also present a way of identifying the location of the peak of the AWG channels by designing two AWGs with 10 nm separation in central wavelength and measure this to be 9.3 nm. The AWG response is also characterized as a function of temperature to make these devices suitable for real-life applications.

The AWGs designed in this work are based on the design technique presented in [10]. Figure 1 shows the input star coupler and the beginning of the waveguide array. The AWG transmission spectrum is simulated using an in-house written algorithm, which uses simulated waveguide mode cross sections, farfield projections across the star coupler, and analytical propagation including phase errors through the arrayed waveguides. First, the design parameters ( $\Delta\lambda$  and  $N_{\text{ch}}$ ) are specified. The two variables in the design are the input waveguide width at the star coupler ( $w_{\text{io}}$ ) and the width of the array waveguides at the start of the star coupler ( $w_{\text{AWG}}$ ). The gap between the array waveguides at the star coupler ( $d_a$ ) is defined by the resolution of the lithography, which in our case is 200 nm. The gap  $d_{\text{io}}$  between the input waveguides is chosen to be equal to  $w_{\text{io}}$  to reduce the sidelobe cross talk. The width of the waveguides in the array ( $w_{\text{AW}}$ ) is chosen such that the phase errors arising from the rough waveguide sidewalls are minimized. We employ a Rowland mounting scheme to reduce the second-order aberrations (defocus) and the third-order aberrations (coma). The radius of the star coupler is calculated as

$$R_a = \frac{s_{\text{max}}}{\theta_{\text{max}}}, \quad \text{where, } s_{\text{max}} = \frac{N_{\text{ch}} - 1}{2} d_{\text{io}}, \quad (1)$$

and  $\theta_{\text{max}}$  is calculated by the intersection of the curve between the electric fields of waveguides  $w_{\text{io}}$  and  $w_{\text{AWG}}$ . The total

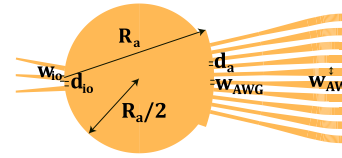


**Fig. 1.** Schematic diagram of an AWG input star coupler and the beginning of the waveguide array showing the various design parameters.

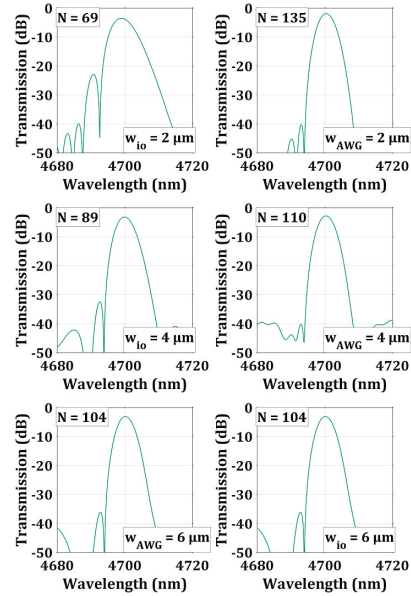


**Fig. 2.** Simulated response of the outermost AWG channel showing the effect of (a)–(c) varying  $w_{\text{io}}$  while keeping  $w_{\text{AWG}}$  fixed at 6  $\mu\text{m}$  and (d)–(f) varying  $w_{\text{AWG}}$  while keeping  $w_{\text{io}}$  fixed at 6  $\mu\text{m}$ . The number of array waveguides for each case is mentioned on top.

number of waveguides in the array is chosen such that 99% light in the star coupler is captured. The design of the AWG is an iterative process and requires the feedback from the layout to ensure that the overall size stays within limits to minimize the phase errors.

Figure 2 shows the simulated transmission of the outermost channel of an eight channel, 200 GHz channel spacing AWG for different values of  $w_{\text{io}}$  and  $w_{\text{AWG}}$ . In Figs. 2(a)–2(c),  $w_{\text{AWG}}$  is kept fixed at 6  $\mu\text{m}$  while  $w_{\text{io}}$  is varied from 2  $\mu\text{m}$  to 6  $\mu\text{m}$ . We see that the sidelobe cross talk decreases as  $w_{\text{io}}$  increases, but this comes at the cost of a large number of array waveguides required to capture 99% of the light transmitted across the star coupler. If we then fix  $w_{\text{io}}$  at 6  $\mu\text{m}$  and vary  $w_{\text{AWG}}$  from 2  $\mu\text{m}$  to 6  $\mu\text{m}$  [Figs. 2(d)–2(f)], we see that  $w_{\text{AWG}}$  and the total number of array waveguides are inversely proportional to each other. The sidelobe cross talk is minimized when  $w_{\text{AWG}}$  is 4  $\mu\text{m}$ . While it seems that increasing  $w_{\text{AWG}}$  would reduce the number of array waveguides even further, it would also increase the chance of coupling into the higher order modes (which is not included in our models) and can cause the device performance to suffer. Therefore, we kept  $w_{\text{io}}$  at 6  $\mu\text{m}$  and  $w_{\text{AWG}}$  at 4  $\mu\text{m}$  for all the AWGs presented in this paper. Another factor that determines the total size of the AWG is the channel wavelength resolution

( $\lambda_{ch}$ ), which is directly proportional to the path length difference ( $\Delta L$ ) between the array waveguides. Increasing  $\Delta L$  obviously increases the total size of the AWG.

The AWGs were fabricated on 100 mm SOI wafers with 1.5  $\mu\text{m}$  thick silicon and 2  $\mu\text{m}$  BOX layers. The bend radius of the fully etched waveguides is 60  $\mu\text{m}$ . Adiabatic bends are used to minimize excess bend loss. The fabrication details and the measured waveguide propagation loss of these waveguides was reported previously in [21] and was found to be  $\sim 1$  dB/cm in the 4.5–4.75  $\mu\text{m}$  wavelength range. The measurement setup used for characterizing the AWGs is reported in [12]. The input/output fibers are opposing each other but have a lateral offset to eliminate stray light coupling in the output fiber.

We designed eight channel AWGs with 200 GHz, 100 GHz, and 50 GHz channel spacing. As the spacing reduces and the resolution increases, the path length difference between the individual array waveguide increases, and hence the AWG size also increases, resulting in phase errors. The path length difference between array waveguides in the AWGs is 26.19  $\mu\text{m}$ , 49.25  $\mu\text{m}$ , and 98.51  $\mu\text{m}$ , respectively. The measured transmission spectra of the AWGs are shown in Figs. 3(a)–3(c). The cross talk of each AWG channel (indicated by the solid squares in the transmission measurements) and the mean 3 dB cross talk are calculated as

$$CXT_x = \frac{\int_{3\text{dB},x} t_{a,x} d\lambda}{\int_{3\text{dB},x} \left( \sum_{y=1}^{N_{cb}} t_{a,y} - t_{a,x} \right) d\lambda},$$

$$\overline{XT} = \frac{1}{N_{cb} - 1} \sum_{x=1}^{N_{cb}} CXT_x, \quad (2)$$

where  $t_i$  is the transmission of the  $i$ th channel. The value of  $\overline{XT}$  for the AWGs increases with resolution and is found to be  $-32.31$  dB,  $-31.87$  dB, and  $-27.28$  dB for 200 GHz, 100 GHz, and 50 GHz, respectively. This increase in the value of  $\overline{XT}$  is expected with the rise in resolution as the size of the AWG increases; however, even for 50 GHz resolution, the measured  $\overline{XT}$  is  $-27.28$  dB, which is comparable to the SOI AWGs reported in the telecom wavelength range. This is a direct consequence of the low phase errors in our low loss waveguides.

The insertion loss is calculated by measuring five straight single mode waveguides on the same chip and normalizing the AWG transmission with respect to the average spectrum. The uncertainty in the insertion loss is estimated to be 33%. The calculated insertion loss for the 200 GHz, 100 GHz, and 50 GHz channel spacing is found to be  $-1.43$  dB,  $-4.2$  dB, and  $-2.3$  dB, respectively. The insertion loss should increase with increasing resolution because of the longer array waveguides. Here, we see that the 100 GHz resolution AWG has a higher insertion loss than both 200 GHz and 50 GHz resolution. This could either be due to local fabrication variations, which could change the waveguide propagation loss between each AWG or due to degradation in facet quality of the coupling waveguides.

Increasing the number of channels is important in several gas sensing applications, as many gases have isotopes that have absorption lines spread across a wavelength range. The bandwidth of the spectrometer also increases for a large number of channels. To detect the isotopes at once using the same device, having a larger number of channels can be beneficial. Increasing the number of channels, however, also causes an increase in the

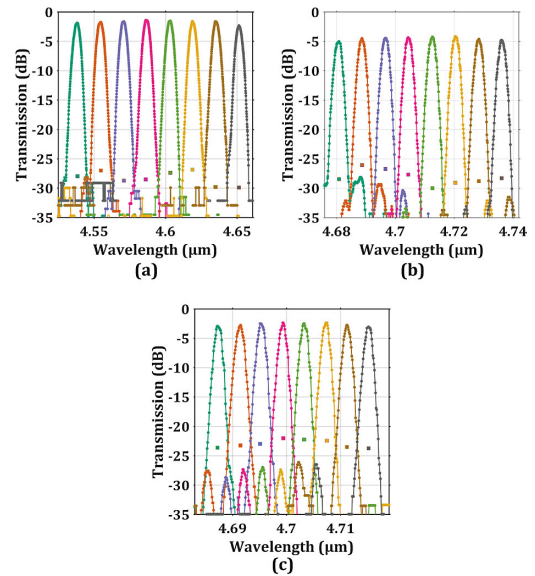


**Fig. 3.** Measured transmission of eight channel AWGs with (a) 200 GHz resolution, (b) 100 GHz resolution, and (c) 50 GHz resolution.

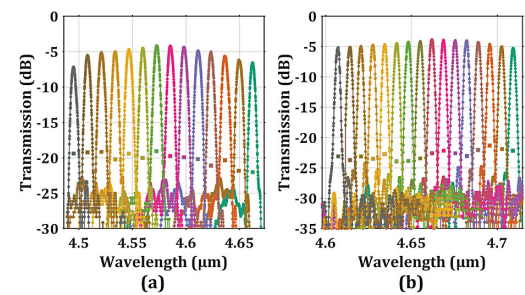


**Fig. 4.** Measured transmission of (a) 14 channel AWGs with 170 GHz resolution and (b) 16 channel AWG with 87 GHz resolution.

AWG size and hence higher cross talk. We designed two AWGs: 14 channels with 170 GHz resolution (119 array waveguides) and 16 channels with 87 GHz resolution (with 137 array waveguides). The measured transmission is shown in Figs. 4(a) and 4(b) with the  $CXT_x$  value shown in solid squares. The calculated value of  $\overline{XT}$  is  $-21.67$  dB for the 14 channel and  $-24.30$  dB for the 16 channel AWG. These values are much higher than the eight channel devices due to added phase errors arising from the increased size of the AWG. The insertion loss for the 14 channel and 16 channel AWG was found to be  $-4.2$  dB and  $-3.8$  dB, respectively. These values are higher than the eight channel 200 GHz and 50 GHz devices because of the increased number of array waveguides.

Unlike other wavelength filters, e.g., ring resonators and MZIs, tuning the response of an AWG is extremely difficult as it would require placing a phase tuning element in each of the array waveguide with potential cross talk between individual phase shifters. The difference in the location of the channel peak between the simulations and the fabricated devices arises due to the differences in the simulated and actual effective index of the waveguides. One way of predicting the channel peak location is to fabricate a series of AWGs with different central channel

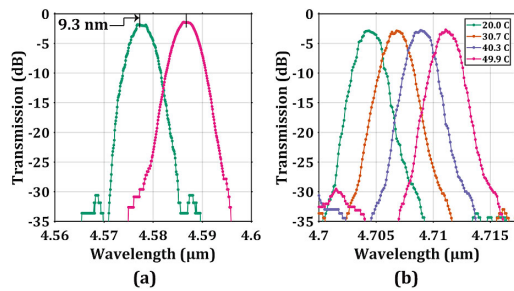


**Fig. 5.** (a) Measured transmission of the central AWG channel for simulated 10 nm channel separation. (b) Measured transmission of the central channel as a function of temperature.

peaks and then characterize them individually. We designed two AWGs with 200 GHz channel spacing and 10 nm difference in the location of central channel peak. Figure 5(a) shows the central channel transmission of both the devices. It can be seen that the difference in the channel peaks is 9.3 nm, which is within 10% of the design parameters.

The location of the AWG peaks is also affected by the temperature. We measured the response of the AWG as a function of temperature, and the results are shown in Fig. 5(b) for the central channel. The peak exhibits a shift of  $0.22 \text{ nm}/^\circ\text{C}$ .

In this Letter, we report AWGs with resolution as high as 50 GHz with eight channels (cross talk  $\overline{XT} = -27.28 \text{ dB}$ , insertion loss  $-2.3 \text{ dB}$ ) and 87 GHz with 16 channels ( $\overline{XT} = -24.30 \text{ dB}$ , insertion loss  $-3.8 \text{ dB}$ ). These results show a remarkable improvement over the previously reported mid-IR AWGs in any material system, and this increased resolution and channel count are essential for their use in spectroscopic systems. The prediction of the channel peak of the fabricated device and the tracking of transmission spectra as a function of temperature make these devices suitable for field applications.

**Funding.** Air Force Research Laboratory (FA8650-15-2-5220); Goddard Space Flight Center; Naval Sea Systems Command (A-19-0461-0001).

**Acknowledgment.** The U.S. Government is authorized to reproduce and distribute reprints for Governmental purposes notwithstanding any copyright notation thereon. The views and conclusions contained herein are those of the authors and should not be interpreted as necessarily representing the official policies or endorsements, either expressed or implied, of AFRL, NASA, NAVSEA, or the U.S. Government.

**Disclosures.** The authors declare no conflict of interest.

## REFERENCES

- X. J. M. Leijtens, B. Kuhlow, and M. K. Smit, *Arrayed Waveguide Gratings* (Springer, 2006), pp. 125–187.
- S. Pathak, D. V. Thourhout, and W. Bogaerts, *Opt. Lett.* **38**, 2961 (2013).
- J. Wang, Z. Sheng, L. Li, A. Pang, A. Wu, W. Li, X. Wang, S. Zou, M. Qi, and F. Gan, *Opt. Express* **22**, 9395 (2014).
- U. Khan, M. Fiers, Y. Xing, and W. Bogaerts, in *Silicon Photonics XV*, G. T. Reed and A. P. Knights, eds. (SPIE, 2020), Vol. **11285**, pp. 161–172.
- N. Ismail, L.-P. Choo-Smith, K. Wörhoff, A. Driessen, A. C. Baclig, P. J. Caspers, G. J. Puppels, R. M. de Ridder, and M. Pollnau, *Opt. Lett.* **36**, 4629 (2011).
- N. A. Yebo, W. Bogaerts, Z. Hens, and R. Baets, *IEEE Photon. Technol. Lett.* **23**, 1505 (2011).
- R. Wang, A. Vasiliev, M. Muneeb, A. Malik, S. Sprengel, G. Boehm, M.-C. Amann, I. Šimonytė, A. Vizbaras, K. Vizbaras, R. Baets, and R. Roelkens, *Sensors* **17**, 1788 (2017).
- A. Stoll, Z. Zhang, R. Haynes, and M. Roth, *Photonics* **4**, 30 (2017).
- M. Muneeb, A. Vasiliev, A. Ruocco, A. Malik, H. Chen, M. Nedeljkovic, J. S. Penades, L. Cerutti, J. B. Rodriguez, G. Z. Mashanovich, M. K. Smit, E. Tourni, and G. Roelkens, *Opt. Express* **24**, 9465 (2016).
- E. J. Stanton, N. Volet, and J. E. Bowers, *Opt. Express* **25**, 30651 (2017).
- A. Malik, M. Muneeb, S. Pathak, Y. Shimura, J. Van Campenhout, R. Loo, and G. Roelkens, *IEEE Photon. Technol. Lett.* **25**, 1805 (2013).
- A. Malik, E. J. Stanton, J. Liu, A. Spott, and J. E. Bowers, *IEEE J. Sel. Top. Quantum Electron.* **24**, 1 (2018).
- P. Barrault, M. Brun, P. Labeye, J.-M. Hartmann, F. Boulila, M. Carras, and S. Nicoletti, *Opt. Express* **23**, 26168 (2015).
- A. Koshkinbayeva, P. Barrault, S. Ortiz, S. Boutami, M. Brun, J. Hartmann, P. Brianceau, O. Lartigue, F. Boulila, R. Orobtcouk, and P. Labeye, *IEEE Photon. Technol. Lett.* **28**, 2191 (2016).
- M. Nedeljkovic, A. V. Velasco, A. Z. Khokhar, A. Delège, P. Cheben, and G. Z. Mashanovich, *IEEE Photon. Technol. Lett.* **28**, 528 (2016).
- F. Pavanello, A. Vasiliev, M. Muneeb, and G. Roelkens, *IEEE Photon. J.* **11**, 1 (2019).
- A. Vasiliev, M. Muneeb, J. Allaert, J. Van Campenhout, R. Baets, and G. Roelkens, *IEEE J. Sel. Top. Quantum Electron.* **24**, 1 (2018).
- M. Montesinos-Ballester, Q. Liu, V. Vakarin, J. M. Ramirez, C. Alonso-Ramos, X. L. Roux, J. Frigerio, A. Ballabio, E. Talamas, L. Vivien, G. Isella, and D. Marris-Morini, *Sci. Rep.* **9**, 14633 (2019).
- J. S. Penadés, A. Sánchez-Postigo, M. Nedeljkovic, A. O.-M. Nux, J. G. Wangüemert-Pérez, Y. Xu, R. Halir, Z. Qu, A. Z. Khokhar, A. Osman, W. Cao, C. G. Littlejohns, P. Cheben, I. Molina-Fernández, and G. Z. Mashanovich, *Opt. Lett.* **43**, 795 (2018).
- S. A. Miller, M. Yu, X. Ji, A. G. Griffith, J. Cardenas, A. L. Gaeta, and M. Lipson, *Optica* **4**, 707 (2017).
- A. Malik, A. Spott, E. J. Stanton, J. D. Peters, J. D. Kirch, L. J. Mawst, D. Botez, J. R. Meyer, and J. E. Bowers, *IEEE J. Sel. Top. Quantum Electron.* **25**, 1 (2019).
- A. Spott, J. Peters, M. L. Davenport, E. J. Stanton, C. D. Merritt, W. W. Bewley, I. Vurgaftman, C. S. Kim, J. R. Meyer, J. Kirch, L. J. Mawst, D. Botez, and J. E. Bowers, *Optica* **3**, 545 (2016).
- E. Stanton, A. Spott, J. Peters, M. Davenport, A. Malik, N. Volet, J. Liu, C. Merritt, I. Vurgaftman, C. S. Kim, J. R. Meyer, and J. E. Bowers, *Photonics* **6**, 6 (2019).